Experimental study of the discharge characteristic in AF-MPDT ignition

IEPC-2019-588

Presented at the 36th International Electric Propulsion Conference,
Vienna, Austria
September 15 – 20, 2019

Yibai Wang[1], Peng Wu[2], Zhiyuan Chen[3], Haibin Tang[4]
Beihang University, Beijing, China, 100191

Abstract: Magnetoplasmadynamic (MPD) thrusters use the Lorentz force from interacting currents and magnetic fields to accelerate the plasma to high speed. In order to provide a desirable magnetic field inside the discharge chamber and so increase the Lorenz force level, the applied-field MPD thrusters (AF-MPDT) were developed. The operating parameters of discharge ignition in the start-up process could be useful for high-power AF-MPDT applications. The ignition tests were carried on and the effect to the discharge characteristic in the start-up process of the working parameters were analyzed, which includes the propellant flow rates, the discharge current flows, the strength of magnetic field produced by the coils and a permanent magnet. The ignition experiments of the water-cooling MAT-50 thruster were successful achieved under three magnetic fields. The electron temperature and ion density using the triple Langmuir probe were measured. The typical signals of discharge voltage were shown. Upon initiation of the power source, there will be an open-circuit voltage between the anode and cathode, the value of which is about 350 V. After ignition, the voltage will decrease rapidly; then the voltage trends to a constant value after a period of oscillation. Arc transition durations under different magnetic field strengths and discharge currents were obtained, and the shortest arc transition duration time is 0.7476s of the model MAT-50-DCEMF. The discharge voltages after arc stabilization generally increase with increasing applied magnetic field strength. The combination influence of discharge current and mass flow rate would be very complex, because too much flow rate or too low discharge current will make start-up phase difficult. The influence degree of cathode flow ratios on start-up phase is no more than 10%.

Nomenclature

Id	=	Discharge current
Ba	=	Applied magnetic field strength generated by coil
$\dot{m}$	=	Total mass flow rate
Vd	=	Discharge voltage
Te	=	Electron temperature
n_i	=	Ion density

[1] Associate professor, School of Astronautics, wangyibai@buaa.edu.cn
[2] Ph.D student, School of Astronautics, 13151149@buaa.edu.cn
[3] Ph.D student, School of Astronautics, @buaa.edu.cn
[4] Professor, School of Space and Environment, thb@buaa.edu.cn

I.Introduction

MAgnetoplasmadynamic (MPD) thrusters are hybrid accelerators with electromagnetic and gas dynamic processes to accelerate plasma, which have considerable potential to enhance future orbit raising of large vehicles, deep space exploration and planetary travel missions for the significant advantages of high specific impulse and thrust density [1,2,3]. Extensive studies have been done to evaluate the steady performance such as thrust, specific impulse and efficiency of steady-state MPD thrusters [4-7], and the effects of discharge current, magnetic field strength, and electrode geometry, etc., on the thrusters' steady performance were discussed. However, studies on the start-up or ignition phase – the prerequisite for steady operation – are far from adequate. Research on the start-up phase of steady-state MPD thrusters was only involved in studies of the cathode erosion, which is regarded as the major life-limiter of MPD thrusters [8-10]. The results show that the start-up phase generally exhibits an erosion rate that is several orders of magnitude higher than that of the steady operation state [11-15]. Though the duration of ignition is quite short (generally several seconds), effects of start-up processes on the plasma thruster are still evident especially when it comes to actual missions or pulsed devices that may involve hundreds of start-ups. Thus, it is crucial to investigate the fundamental processes underlying the ignition phase.

In the previous studies, experiments with 30-50 runs under different preset ignition currents were performed to determine the average erosion rate during the start-up phase of a steady-state self-field MPD (SF-MPD) thruster [11]. A typical current-voltage plot of the initial starting phase and the start-up phase duration as a function of ignition current were presented. In another study on the cathode phenomena of SF-MPD thrusters, experiments with single ignitions and series ignitions were performed [16]. The ignition phase was believed to be characterized by a cold cathode and a highly unstable, spotty arc attachment. Besides, the start-up phase ends when the cathode is hot enough for thermionic emission to support the current demand, indicated by a sudden decrease in discharge voltage together with an increase in discharge current.

Compared with SF-MPD thrusters, the applied-field MPD (AF-MPD) thrusters using magnetizing coils or permanent magnets to create a steady longitudinal magnetic field. The additional B field improves the performances of MPD thrusters at power level from 10 to 200 kW. Unfortunately, despite of previous studies [13, 16] involving analyzing the ignition processes of SF-MPD thrusters, investigations on the start-up phase of steady-state applied-field MPD (AF-MPD) thrusters are still insufficient and the effects of working parameters on the start-up characteristics need to be further investigated.

In a recent experimental study of a pulsed, quasi-steady, 100 kW-class AF-MPD thruster, Albertoni et al. [17] found that the cathode current attachment mainly distributed at the external surface of the electrode during the arc ignition phase, and a transition from diffuse to hollow cathode behavior was observed after approximately 400 ms from the breakdown. Localized arc attachments turned out to be critical in the operation range tested in their study, but no detailed investigations on the start-up processes were made.

The purpose of this paper is to investigate the ignition processes of an AF-MPD thruster (MAT-50) at three kind of magnetic fields and to analyze the effects of important factors, such as magnetic field, mass flow rates and discharge current on its start-up characteristics. Furthermore, instead of evaluating the cathode erosion rate, this work mainly focuses on the transient feature of the start-up phase of AF-MPD thrusters by comparing the arc transition durations under different operation conditions.

II.Experimental Facility

A. Vacuum System

The vacuum system consists of a vacuum tank, three class of pumping system, electrical control equipment and other peripheral equipment. The size of the vacuum tank is Φ2.5m×5m. The pumping system consists of four SV-300 mechanical vacuum pumps, a ZJP-1200 Roots pumps and two JK-900 high vacuum oil diffusion pumps. The system achieves an ultimate vacuum of 1.0×10^{-4} Pa with total pump speed over 64000L/s, and the environment pressure can be maintained under 1.0×10^{-1} Pa when the (argon) propellant mass flow rate is lower than 40mg/s.

B. Power Source System

The power source system provides a high voltage pulse to ignite the thruster, provides power for the thruster to accelerate the plasma, and provides power for the magnetic field coils to sustain the external magnetic field. The power source system consists of an ignition power source, a thruster power source, a coil power source and cables. The ignition power input was provided by a current-regulated power supply, which consists of a main circuit, control circuit, safety circuit, and high-frequency starter circuit. The starter circuit could output a 10kV pulse at a frequency of 40-1000 kHz to initiate the arc, and the open-circuit voltage of the power supply is about 340 V. Besides, the maximum current output of the thruster's power supply is 350 A and the maximum voltage is 100 V.

The water-cooling system can provide high-pressure 295K water flow to exchange the heat of the thruster, the magnetic coils and power sources. This system consists of pumps group, the water tank, the compressor, the water supply pipelines and the pumps controllers.

C. Thruster MAT-50

As shown in Figure 1, The MAT-50 used in this study has a central hollow cathode made of tungsten (99.9%) and a flat copper anode which has a water-cooling structure to exchange the heat from the anode surface and protect the permanent magnet. The anode assembly consists of three parts connected by bolts, and the graphite is used for sealing. The anode has an inner and outer diameter of 46 and 107 mm, respectively, and is 50 mm long. Propellant is injected into the discharge chamber via the hollow cathode and the ring channel between the insulator and anode connection component, and the mass flow rate was controlled and measured by mass flow controllers. The cathode is 30 mm long (inside the discharge chamber) and 16 mm in diameter, and is held in place by a water-cooled copper structure. There are seven channels in cathode, and each channel is 1.7 mm in diameter. The insulator between anode and cathode is made of boron nitride. Other insulation parts are realized with PEEK.

In order to improve the performance of AF-MPDT, a permanent magnet was placed in the anode water-cooling chamber in this paper. As shown in Figure 1, the magnetic field of permanent magnet is quite different with coil. The N40RbFeB permanent magnet has an inner and outer diameter of 62 and 78 mm, and is 25 mm long.

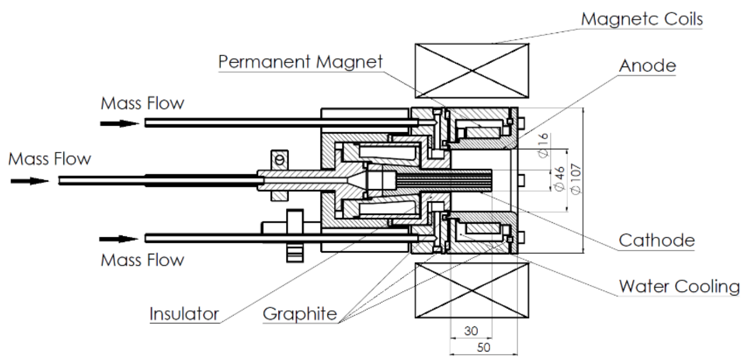

Figure 1. Schematic diagram of model MAT-50.

D. Acquisition System and Langmuir Probes

A sixteen-isolated-channel data acquisition system was used in this study to collect the discharge voltage, the discharge current, and the propellant mass flow rate data during the tests, and the sampling rate was 1 kHz in all the tests.

To measure the electron temperature and ion density, the triple Langmuir probe method was used in the experiments, which is different from the classical single and double Langmuir probe diagnostics as it does not require any voltage and frequency sweeps [18]. The triple Langmuir probe consists of three separate single Langmuir probes. One is positive, the second one is floating and the third one is negative. It floats as a whole. The measurements of the voltage difference Vd_2 (between the positive and floating probes) and loop current I_3 (between the positive and negative probes) versus discharge time could display the time-resolved electron temperature and density respectively [19].

The triple Langmuir probe consists of three tungsten wires, each of 0.3 mm diameter, and possesses a 6.4 mm long exposed tip as the collecting conductor. These wires are configured in a regular triangle fashion, with their axis aligned with the arc generator centerline. The intervals between the wires are of 2 mm, which is far larger than the ion sheath (1.49×10^{-3} mm) around the probe, this way the probes do not disturb each other. In our diagnostic circuit, Vd_3 is fixed at 40V provided by a 70V, 3 A power supply. The loop current I_3 is measured as the voltage drop from a 1000 Ω shunt. The simultaneous probe voltage difference Vd_2, loop current I_3 were also obtained by the data acquisition system in the experiments. Probe positioning was maintained by a two-axis translation mechanism powered by two step-motors. The mechanism consists of two movement stands inside the vacuum chamber, and two servo control windows outside the vacuum chamber.

III. Results and Discussion

A. Magnetic field Variation of MAT-50

If we do not install the permanent magnet, the magnetic field is generated only by the coils, like other AF-MPD thrusters and the model is named MAT-50-NP. Benefiting from the interaction between the external magnetic coils and the permanent magnet, there are two opposite direction of magnetic lines in permanent magnet, which means that two different distributions may be formed when the direction of coils is changed: discharge chamber enhanced magnetic field (DCEMF) and magnetic nozzle enhanced magnetic field (MNEMF). The magnetic strength distribution of MAT-50-NP, MAT-50-DCEMF and MAT-50-MNEMF are shown in Figure 2. The magnetic field of MAT-50-DCEMF and MAT-50-MNEMF are quite different with MAT-50-NP. A convergent-divergent-convergent (C-D-C) magnetic field is formed in MAT-50-MNEMF, and D-C one is formed in MAT-50-DCEMF. In the MAT-50-MNEMF, the magnetic strength is increased 0.015T at the exit of the thruster and decreased 0.08T at cathode tip, which is opposite in the MAT-50-DCEMF.

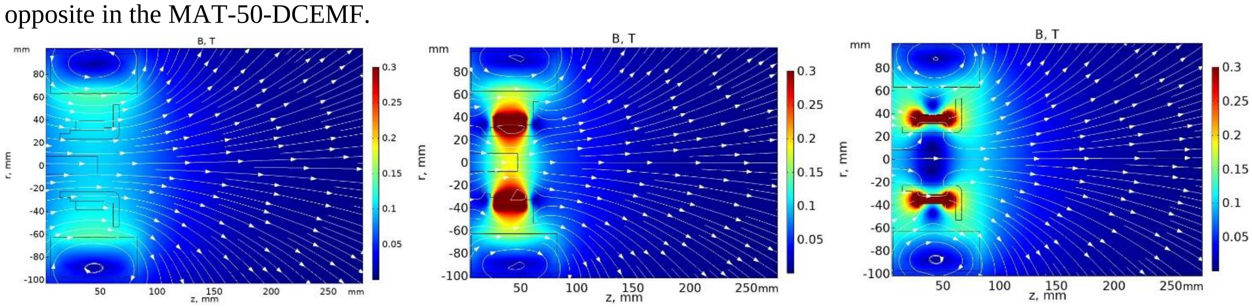

(a) MAT-50-NP (b) MAT-50-DCEMF (c) MAT-50-MNEMF

Figure 2. Magnetic strength distribution of three models.

B. Scheme of Ignition Tests

A series of ignition tests have been conducted with argon under different magnetic field strengths and discharge currents, and the ignition tests scheme are listed in Table 1. The electron temperature, ion density and discharge voltage are measured in part 1 and part 3. Only the discharge voltage is measured in part 2.

Table 1 Scheme of ignition tests

<table>
<tr><td rowspan="4">Part 1
(Id=150A, $\dot{m} = 42$mg/s)</td><td>Magnetic Field</td><td colspan="12">Ba(mT)</td></tr>
<tr><td>MAT-50-NP</td><td colspan="4" rowspan="3">75</td><td colspan="4" rowspan="3">100</td><td colspan="4" rowspan="3">125</td></tr>
<tr><td>MAT-50-DCEMF</td></tr>
<tr><td>MAT-50-MNEMF</td></tr>
<tr><td rowspan="4">Part 2
(MAT-50-NP, Ba=125 mT)</td><td>Id</td><td colspan="12">$\dot{m}$ (mg/s)</td></tr>
<tr><td>150A</td><td colspan="3" rowspan="3">21</td><td colspan="3" rowspan="3">25.2</td><td colspan="3" rowspan="3">33.6</td><td colspan="3" rowspan="3">42</td></tr>
<tr><td>175A</td></tr>
<tr><td>200A</td></tr>
<tr><td rowspan="2">Part 3
(Id=150A, Ba=125 mT)</td><td>Magnetic Field</td><td colspan="12">Cathode Flow to Total Flow Ratio ($\dot{m} = 42$mg/s)</td></tr>
<tr><td>MAT-50-DCEMF</td><td colspan="2">0.2</td><td colspan="2">0.4</td><td colspan="2">0.5</td><td colspan="2">0.6</td><td colspan="2">0.8</td><td colspan="2">1.0</td></tr>
</table>

C. Arc Transition Duration

The initial operating condition was: *Id*=150A, *Ba*=100mT, $\dot{m}$=42mg/s, Figure 3 (a) depicts the typical discharge voltage during the start-up phase of the thruster MAT-50-NP. Similar to that in an arcjet [19, 20], the start-up phase of thruster MAT-50-NP can be characterized by three steps, i.e., arc initiation, arc transition, and arc stabilization. The arc initiation step is featured by a sudden decrease in discharge voltage and an increase in discharge current when a high-frequency pulse is exerted between the cathode and anode. During this stage, initial localized tiny spots are formed on the cathode, and the propellant injected into the discharge chamber is drastically ionized by electrons emitted from these spots. During the arc transition step, whose duration may be affected by applied magnetic field strength, highly unstable arc spots remain on the cathode surface, accompanied by fluctuations of the discharge voltage and current. These fluctuations tend to disappear when the cathode becomes hot enough for thermionic emission to support current conductions, indicating the establishment of a stable diffuse arc attachment and the end of the start-up phase.

For the Model MAT-50-NP, transition time of arc lasted 3.6761s. After ignition, the voltage decreased rapidly; then the voltage trend to a constant value (near 100V) after a period of oscillation. Furthermore, arc transition durations under different magnetic field strengths and discharge characteristic at the same ignition condition are presented in Figure 3 (b) and (c).

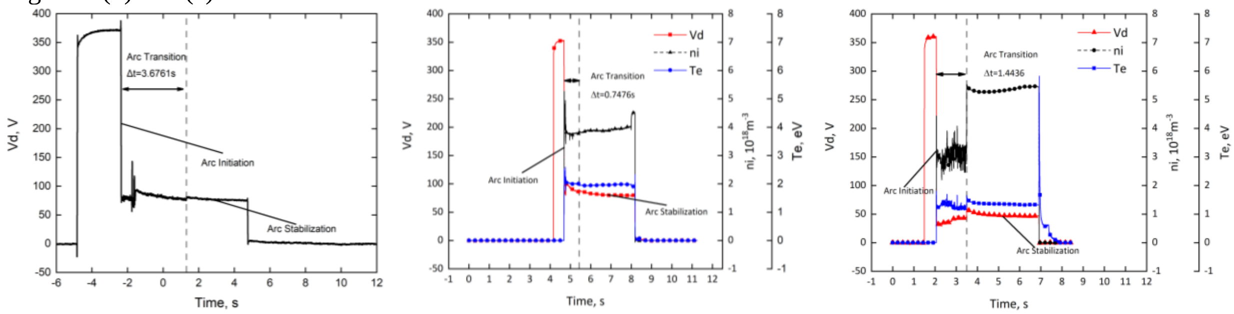

(a) MAT-50-NP (b) MAT-50-DCEMF (c) MAT-50-MNEMF

Figure 3. Typical discharge voltage and transition curves.

As known from Figure 2, the model MAT-50-DCEMF has the largest magnetic field intensity distribution in the discharge chamber. Figure 3(b) show that the arc transition duration is affected by magnetic field intensity. With the increase of magnetic field intensity, the duration time decreases to 0.7476s, which indicates that the condition of strong magnetic field is beneficial to start-up process. In MAT-50-MNEMF, although the magnetic field strength in the cathode tip region decreases a little, the average magnetic field intensity of the whole discharge chamber especially in the magnetic nozzle region is still higher than that of the model MAT-50. In Figure 3(c), the duration time of MAT-50-MNEMF is also shorter than that of model MAT-50. The measurement curves of electron temperature and ion density show the same characteristics as discharge voltage.

As can be seen in Figure 3(c), the arc transition duration fluctuates with applied magnetic field strength, indicating two opposite effects of the applied magnetic field strength on the arc transition processes. The application of magnetic field can accelerate the arc transition processes by increasing the input power and speeding up the heating of the cathode; moreover, magnetic field can also lead to more regular spot movements into the retrograde direction, thus accelerating the diffusion of hot spots and facilitating the transition from spotty arc attachments to diffuse ones. Nevertheless, magnetic field may obstruct the arc transition processes by confining plasma to the centerline and causing the starvation of charged particles that can conduct currents near the anode. The interactions of these two opposite effects result in the fluctuations of the arc transition duration.

D. Discharge Voltage after Arc Stabilization

Discharge voltages, electron temperature and ion density after arc stabilization of each test were recorded, as depicted in Figure 4. We can see that the three parameters generally increase with increasing applied magnetic field strength. This is because the confinement of plasmas tends to be stronger with larger magnetic field strength, causing more severe starvation of current-conducting particles near the anode and a decrease of the radial conductivity of plasma. Moreover, the increase of the discharge voltage also implies that more energy will be input into the thruster with larger magnetic field strength, which will speed up the heating of electrodes and accelerate the arc transition processes.

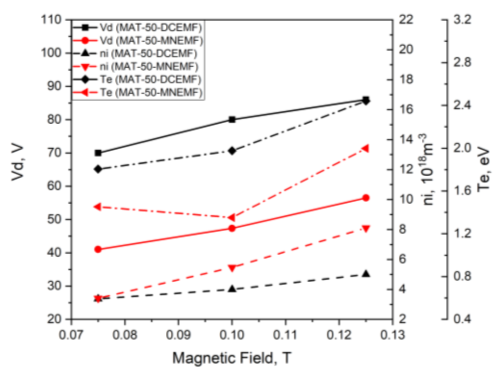

Figure 4. Variation of Parameters in Arc stabilization with different *Ba*.

Figure 5 shows the Influence of discharge current and propellant mass flow rate on start-up phase when the applied field Ba=125mT of the model MAT-50. The discharge current can be varied from 150A to 200A, and the propellant mass flow rate can be varied from 21mg/s to 42mg/s. Under the same discharge current and magnetic field conditions, the discharge voltage decreases with the increase of mass flow rate. More specifically, gas dynamic effects tend to be more evident at higher mass flow rate and may affect the effects of magnetic field strength on the discharge voltage. As seen in Figure 5(b), the duration time of arc transition are more complex, because too much flow rate or too little discharge current will make start-up phase difficult to ignition. All of these phenomena are in accordance with the discussions about the ignition test results and arc transition durations above.

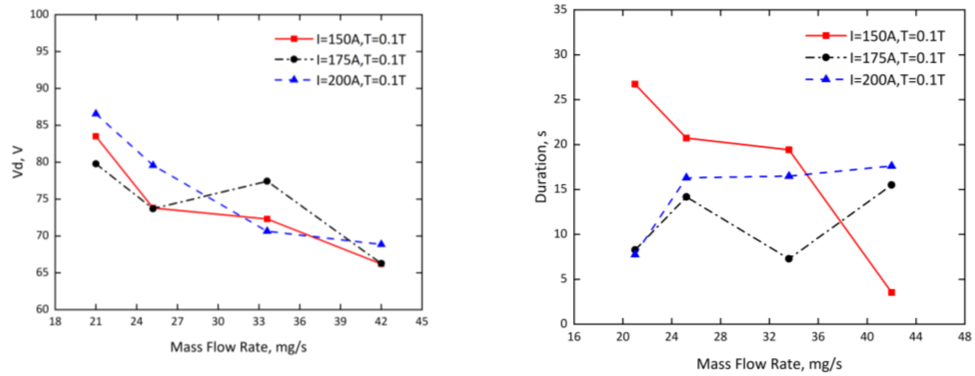

(a) Discharge voltage (b) Duration time of arc transition

Figure 5. Discharge voltages and arc transition under different $\dot{m}$.

A part of propellant enters the discharge chamber from the multiple central holes of the hollow cathode, which can improve the thermal effect and prolong the service life of the cathode. There is a large cavity inside the cathode base connecting with seven narrow cylindrical channels. The cavity acts as a buffer to increase the uniformity of the propellant distribution in seven channels. How to distribute the cathode intake flow ratio also affects the start-up of thruster ignition? Figure 6 shows variation of parameters in arc stabilization with different cathode flow ratios. It can be seen that the ratio between 0.4 and 0.5 is appropriate, too large or too small will have a slight impact on start-up characteristics. But in general, the degree of influence is less than 10%.

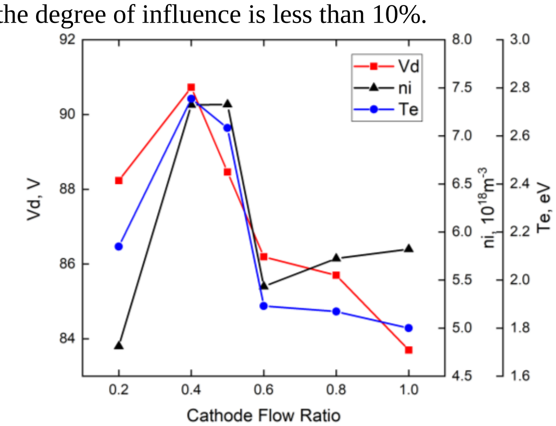

Figure 6. Arc stabilization with different cathode flow ratio.

IV.Conclusion

Experimental investigations have been carried out to analyze the ignition processes of a steady-state water-cooling MAT-50 thruster, and to clarify the influence of applied magnetic field strength and other working conditions on these processes. Benefiting from the interaction between the external magnetic coils and the permanent magnet, the typical signal of discharge voltage, electron temperature and ion density after arc stabilization of each test were obtained under three magnetic field strength distributions. Successful ignitions were achieved when external magnetic field was applied, implying that applied magnetic field can contribute to the breakdown of neutral gas and the establishment of arcs. Upon initiation of the power source, there will be an open-circuit voltage between the anode and cathode. The shortest arc transition duration time is 0.7476s of the model MAT-50-DCEMF.

The characteristic parameters after arc stabilization generally increase with increasing applied magnetic field strength. This represents greater plasma confinement and higher input energy under larger applied magnetic field strength, thus verifying the discussions about the ignition test results and arc transition durations. The combination influence of discharge current and mass flow rate would be very complex, because too much flow rate or too little discharge current will make start-up phase difficult. The optimal distribution ratio of cathode mass flow to total mass flow is between 0.4 and 0.5, and the degree of influence on start-up phase is no more than 10%. In the future we will focus on the characteristics of arc transition fluctuation during ignition under different working conditions.

Acknowledgments

This work was supported by the Advance Research Projects of Civil Aerospace Technology Program and the National Natural Science Foundation of China (Grant No. 11872093).

References

The following pages are intended to provide examples of the different reference types. You are not required to indicate the type of reference; different types are shown here for illustrative purposes only.

[1]Herdrich, G., Boxberger, A., Petkow, D., Gabrielli, R. A., Fasoulas, S., Andrenucci, M., Albertoni., R., Paganucci, F., and Rossetti, P., "Advanced Scaling Model for Simplified Thrust and Power Scaling of an Applied-Field Magnetoplasmadynamic Thruster," *46th AIAA/ASME/SAE/ASEE Joint Propulsion Conference and Exhibit*, AIAA, Washington, DC, 2010, pp., 1-19.

[2]Paganucci, F., Rossetti, P., Andrenucci, M., Tikhonov, V. B., and Obukhov, V. A., "Performance of an Applied Field MPD Thruster with a Pre-ionization Chamber," *33rd Plasmadynamics and Lasers Conference*, AIAA, Washington, DC, 2002, pp., 1-10.

[3]Tahara, H., Kagaya, Y., and Yoshikawa, T., "Effects of Applied Magnetic Fields on Performance of a Quasisteady Magnetoplasmadynamic Arcjet," *Journal of Propulsion and Power*, Vol. 11, No. 2, 1995, pp. 337-342.

[4]Myers, R. M., Mantenieks, M, Sovey, J., "Geometric Effects in Applied-Field MPD Thrusters," *AIAA/DGLR/JSASS 21st International Electric Propulsion Conference*, AIAA, Washington, DC, 1990, pp., 1-18.

[5]Kodys, A. D., and Choueiri, E. Y., "A Critical Review of the State-of-the-Art in the Performance of Applied-field Magnetoplasmadynamic Thrusters," *41st AIAA/ASME/SAE/ASEE Joint Propulsion Conference and Exhibit*, AIAA, Washington, DC, 2005, pp., 1-23.

[6]Mikellides, P. G., Turchi, P. J., and Roderick, N. F., "Applied-Field Magnetoplasmadynamic Thrusters, Part 1: Numerical Simulations Using the MACH2 Code," *Journal of Propulsion and Power*, Vol. 16, No. 5, 2000, pp., 887-893.

[7]Boxberger, A., Bambach, P., Herdrich, G., Fasoulas, S., Merino, M., and Ahedo, E., "Experimental Investigation of Steady-State Applied-Field Magnetoplasmadynamic Thrusters at Institute of Space Systems," *48th AIAA/ASME/SAE/ASEE Joint Propulsion Conference & Exhibit*, AIAA, Washington, DC, 2012, pp., 1-10.

[8]Rowe, R., Jaskowsky, W. V., Clark., K, and Jahn, R., "Erosion Measurements on Quasi-Steady MPD Thrusters," *AlAA/JSASS/DGLR 15th International Electric Propulsion Conference*, AIAA, New York, 1981, pp., 1-8.

[9]Polk, J. E., Jaskowsky, W. V., Kelley, A. J., and Jahn, R. G., "Measurement of MPD Thruster Erosion Using Surface Layer Activation," *Journal of Propulsion and Power*, Vol. 3, No. 1, 1987, pp., 33-38.

[10]Sovey, J. S., and Mantenieks, M. A., "Performance and Lifetime Assessment of Magnetoplasmadynamic Arc Thruster Technology," *Journal of Propulsion and Power*, Vol. 7, No. 1, 1991, pp., 71-83.

[11]Schrade, H. O., Auweter-Kurtz, M., and Kurtz, H. L., "Cathode Phenomena in Plasma Thrusters," *AlAA/JSASS/DGLR 19th International Electric Propulsion Conference*, AIAA, New York, 1987, pp., 1-8.

[12]Myers, R. M., Suzuki, N., Kelley, A. J., and Jahn, R. G., "Cathode Phenomena in a Low Power, Steady State MPD Thruster," *24th AIAA/ASME/SAE/ASEE Joint Propulsion Conference and Exhibit*, AIAA, Washington, DC, 1988, pp., 1-25.

[13]Schrade, H. O., Auweter-Kurtz, M., and Kurtz, H. L., "Cathode Erosion Studies on MPD Thrusters," *AIAA Journal*, Vol. 25, No. 8, 1987, pp., 1105-1112.

[14]Andrenucci, M., Paganucci, F., and La Motta, G., "MPD Thruster Performance with Cathode Heating," *28th AIAA/ASME/SAE/ASEE Joint Propulsion Conference and Exhibit*, AIAA, Washington, DC, 1992, pp., 1-7.

[15]Polk, J. E., Kelley, A. J., Jahn, R. G., Kurtz, H. L., Auweter-Kurtz, M., and Schrade, H. O., "Mechanisms of Hot Cathode Erosion in Plasma Thrusters," *AlAA/ DGLR / JSASS 21st International Electric Propulsion Conference*, AIAA, Washington, DC, 1990, pp., 1-20.

[16]Auweter-Kurtz, M., Glocker, B., Kurtz, H. L., Loesener, O., Schrade, H. O., Tubanos, N., Wegmann, T., Willer, D., and Polk, J. E., "Cathode Phenomena in Plasma Thrusters," *Journal of Propulsion and Power*, Vol. 9, No. 6, 1993, pp., 882-888.

[17]Albertoni, R., Paganucci, F., Rossetti, P., and Andrenucci, M., "Experimental Study of a Hundred-Kilowatt-Class Applied-Field Magnetoplasmadynamic Thruster," *Journal of Propulsion and Power*, AIAA Early Edition, 2013, pp. 1-8.

[18]Chen, S. L. and Sekiguchi, T., "Instantaneous direct-display system of plasma parameters by means of triple probe," *Journal of Applied Physics*, vol. 36, no. 8, 1965, pp., 2363–2375.

[19]Zhang, Z., Tang, H., Kong, M., Kitaeva, A., Zhang, Z. and Cao S., "Temporal Evolution and Spatial Distribution of the Plume Plasma from an MPD Arc Generator," *IEEE TRANSACTIONS ON PLASMA SCIENCE*, vol. 46, no. 8, 2018, pp., 2901–2908.